

Impacts of Meteorological Uncertainties on the Haze Formation in Beijing-Tianjin-Hebei (BTH) during Wintertime: A case study

Naifang Bei¹, Jiarui Wu², Miriam Elser³, Tian Feng², Junji Cao², Imad El-Haddad³, Xia Li², Rujin Huang², Zhengqiang Li⁴, Xin Long², Li Xing², Shuyu Zhao², Xuexi Tie², André S. H. Prévôt³, and Guohui Li^{2*}

¹School of Human Settlements and Civil Engineering, Xi'an Jiaotong University, Xi'an, Shaanxi, China

²Key Lab of Aerosol Chemistry and Physics, SKLLQG, Institute of Earth Environment, Chinese Academy of Sciences, Xi'an, China

³Laboratory of Atmospheric Chemistry, Paul Scherrer Institute, 5232 Villigen, Switzerland

⁴State Environmental Protection Key Laboratory of Satellite Remote Sensing, Institute of Remote Sensing and Digital Earth, Chinese Academy of Sciences, Beijing, China

*Correspondence to: Guohui Li (ligh@ieecas.cn)

Abstract: In the present study, a persistent heavy haze episode from 13 to 20 January 2014 in Beijing-Tianjin-Hebei (BTH) is simulated using the WRF-CHEM model through ensemble simulations to investigate impacts of meteorological uncertainties on the haze formation. Model results show that uncertainties in meteorological conditions substantially influence the aerosol constituent simulations at an observation site in Beijing, and the ratio of the ensemble spread to ensemble mean (RESM) exceeds 50%. The ensemble mean generally preforms well in reproducing the fine particles (PM_{2.5}) temporal variations and spatial distributions against measurements in BTH. The meteorological uncertainties do not alter the PM_{2.5} distribution pattern in BTH principally or dominate the haze formation and development, but remarkably affect the simulated PM_{2.5} level, and the RESM for the simulated PM_{2.5} concentrations can be up to 30% at the regional scale. In addition, the rather large RESM in PM_{2.5} simulations at the city scale also causes difficulties in evaluation of the control strategies. Therefore, our results suggest that the ensemble simulation is imperative to take into account the impact of the meteorological uncertainties on the haze prediction.

1 Introduction

Over the past three decades, rapid industrialization and urbanization have caused severe air pollution in China, particularly during wintertime heavy haze with extremely high levels of fine particles ($PM_{2.5}$) frequently engulfs the north of China (e.g., Chan and Yao, 2008; Fang et al., 2009; Zhao et al., 2013; Huang et al., 2014; Guo et al., 2014; Wu et al., 2017; Li et al., 2017). Elevated atmospheric aerosols or $PM_{2.5}$ not only influence the Earth climate system, but also remarkably impair visibility and potentially cause severe health defects (e.g., Penner et al., 2001; Pope and Dockery, 2006; Zhang et al., 2007).

Meteorological condition is critical for understanding the formation, transformation, diffusion, transport, and removal of the pollutants in the atmosphere. Dabberdt et al. (2004) have listed the meteorological research needs for improving air quality forecasting, one of which is to provide the model uncertainty information through ensemble prediction capabilities and quantify uncertainties and feed-backs between meteorological and air quality modeling components. Numerous studies have been performed in China to explore the role of meteorological conditions in the air pollution formation (e.g., Gao et al., 2011; Zhang et al., 2012; Wu et al. 2013; Wang et al. 2014; Zhang et al. 2015; Bei et al. 2016a, b). Most recently, Liu et al. (2017) have investigated the meteorological impacts on the $PM_{2.5}$ concentrations over Beijing-Tianjin-Hebei (BTH) in December 2015. Their results have demonstrated that the unfavorable meteorological conditions are the main reason for deterioration of the air quality in BTH, while the undertaken emission control measures have only mitigated the air pollution slightly.

Previous studies on the air quality forecasting sensitivity to meteorological uncertainties mainly include Monte Carlo simulations (e.g. Dabberdt and Miller, 2000; Beekmann and Derognat, 2003) and adjoint sensitivity studies (e.g. Menut, 2003). The ensemble approach has also been applied to photochemical and secondary organic aerosol

(SOA) simulations in various numerical models (e. g. Galmarini et al., 2004; McKeen et al., 2005), photo-chemical reactions (e. g. Delle Monache and Stull, 2003), emission scenarios (e. g. Delle Monache et al., 2006), physical parameterizations (e. g. Mallet and Sportisse, 2006), and meteorological initial conditions (e. g. Zhang et al. 2007; Bei et al. 2012). The ensemble means have generally performed better than most of individual models. Uncertainties in meteorological initial conditions have been shown to substantially influence both ozone (O₃) and SOA simulations, including the peak time concentrations, the horizontal distributions, and the temporal variations (Zhang et al. 2007; Bei et al. 2012). Recently, Sharma et al. (2016) have evaluated uncertainties in surface O₃ simulations over the South Asian region during the pre-monsoon season due to different emission inventories and different chemical mechanisms. They have suggested that the assessment of the tropospheric O₃ budget and its implications on public health and agricultural output should be conducted prudently considering the huge uncertainties caused by emission inventories and chemical mechanisms. Solazzo et al. (2017) have emphasized the high interdependencies among meteorological and chemical variables and the related errors, indicating that the evaluation of the air quality model performance needs to be confirmed by more complementary analysis of meteorological fields and chemical precursors.

The purpose of the present study is to explore impacts of the uncertainties in meteorological conditions on the PM_{2.5} simulations or forecasts in BTH through ensemble simulations using the WRF-CHEM model. The methodology and model are presented in Section 2. The analyses, results, and discussions are included in Section 3. The summary and conclusions are given in Section 4.

2 Model and Methodology

2.1 WRF-CHEM Model

A specific version of the WRF-CHEM model is used to examine impacts of the uncertainties in meteorological conditions on the PM_{2.5} simulations or the haze formation in BTH, which is developed by Li et al. (2010; 2011a, b; 2012) at the Molina Center for Energy and the Environment. The model includes a new flexible gas phase chemical module and the CMAQ/Models-3 aerosol module developed by US EPA (Binkowski and Roselle, 2003). The inorganic aerosols are predicted using the ISORROPIA Version 1.7 (Nenes et al., 1998). The SOA formation is simulated using a non-traditional SOA module, including the volatility basis-set (VBS) modeling method and the SOA contributions from glyoxal and methylglyoxal. Detailed description of the WRF-CHEM model can be found in Li et al. (2010; 2011a, b; 2012). A persistent heavy haze pollution episode from 13 to 20 January 2014 in BTH is simulated. The model simulation domain is shown in Figure 1, and detailed model configurations can be found in Table 1.

2.2 Ensemble Initialization Method

The ensemble initialization method used in the present study is called “climatological ensemble initialization method” (Zhang et al., 2007; Bei et al., 2012). In the approach, dynamically consistent initial and boundary conditions are statistically sampled from a seasonal meteorological data set. In order to represent the wintertime climatological statistics, a data set during the period from 1 November 2013 to 28 February 2014 is generated using NCEP-FNL 1°×1° reanalysis data. The perturbed variables include the horizontal wind components, potential temperature, perturbation pressure, and mixing ratio of water vapor. Other prognostic variables such as vertical velocity and mixing ratios of hydrometeors are not perturbed. In general, the perturbation in horizontal wind components constitutes the most important uncertainty in those variables (Bei et al., 2008; 2010). Thirty ensemble members are randomly chosen from this climatological data set. Similarly, boundary conditions for each ensemble member are generated from the same data set beginning at the randomly

selected initial time of the given member, and extended for the same length of time as the simulated episode. Deviations of the initial and boundary condition data for each member from the climatological mean for the entire period are then scaled down to 20% to reduce the ensemble spread to be less than typical observation error magnitudes (Nielsen-Gammon et al., 2007) and added to the unperturbed initial and boundary conditions derived directly from the NCEP-FNL analyses valid at 12:00 UTC on 12 January 2014, which are used for the 6-km domain ensemble simulation. Figures 2a–d show the vertical distribution of the average initial ensemble spread which is calculated as the standard deviation of the perturbations imposed on each ensemble member's initial field. The average spread is 0.5–3.0 m s⁻¹ for horizontal winds (U and V component), 0.5–1.1 K for temperature, 0.02–0.48 hPa for pressure, and 0–0.15 g kg⁻¹ for the water vapor mass mixing ratio. The initial ensemble spreads of meteorological variables are generally less than their typical observation error magnitudes. It is worth noting that all the ensemble simulations used the same initial and boundary conditions for chemical fields, as well as the same anthropogenic emission inventory.

2.3 Pollutants Measurements

The hourly near-surface CO, SO₂, NO₂, O₃, and PM_{2.5} mass concentrations in BTH are released by the China's Ministry of Environmental Protection (China MEP) and can be downloaded from the website <http://www.aqjstudy.cn/>. The Aerodyne High Resolution Time-of-Flight Aerosol Mass Spectrometer (HR-ToF-AMS) with a novel PM_{2.5} lens is used to measure the sulfate, nitrate, ammonium, and organic aerosols (OA) from 9 to 26 January 2014 at the Institute of Remote Sensing and Digital Earth (IRSDE), Chinese Academy of Sciences (40.00°N, 116.38°E) in Beijing (Figure 1) (Williams et al., 2013). The Positive Matrix Factorization (PMF) technique is utilized with constraints implemented in SoFi (Canonaco et al., 2013) to analyze the sources of OA and five components are separated by

their mass spectra and time series. The components include hydrocarbon-like OA (HOA), cooking OA (COA), biomass burning OA (BBOA), coal combustion OA (CCOA), and oxygenated OA (OOA). HOA, COA, BBOA, and CCOA are interpreted for surrogates of primary OA (POA), and OOA is a surrogate for SOA. Detailed information about the HR-ToF-AMS measurements and data analysis can be found in Elser et al. (2016). A Lidar has also been deployed at IRSDE and the aerosol backscatter signal is used to retrieve the planetary boundary layer (PBL) height.

3 Results and Discussions

3.1 Synoptic Overview

Figure 3 shows temporal evolutions of the observed $PM_{2.5}$ mass concentrations averaged over 13 cities (see Figure 1) in BTH during the severe haze episode from 13 to 21 January 2014. The observed $PM_{2.5}$ mass concentrations are frequently higher than $250 \mu g m^{-3}$ in the 13 cities during the episode, exceeding the standard of severe pollutions (hourly $PM_{2.5}$ mass concentration exceeding $250 \mu g m^{-3}$, Feng et al., 2016). The haze in BTH was in the stage of development from January 13 to 15, with the gradual increase of the $PM_{2.5}$ concentration. BTH was most polluted when the haze was in the maturity stage on January 16, with the $PM_{2.5}$ concentration exceeding $400 \mu g m^{-3}$ in most of the cities. From January 17 to 19, the $PM_{2.5}$ concentrations fluctuated considerably, which was primarily caused by the transition between different synoptic situations. During nighttime on January 19, the haze in BTH rapidly dissipated, with the $PM_{2.5}$ concentration decrease of several hundreds of $\mu g m^{-3}$ in two or three hours. In addition, the diurnal cycles of the observed $PM_{2.5}$ mass concentrations were not clear, demonstrating the obvious regional pollution characteristics in BTH. For the four mega-cities in BTH, the $PM_{2.5}$ levels in Shijiazhuang and Baoding were

much higher than Beijing and Tianjin, which is caused by the massive local emissions in Shijiazhuang and Baoding.

NCEP-FNL reanalysis data is used to examine the effect of synoptic conditions on the air pollution during the haze episode in BTH. Figures s1-s3 show the synoptic conditions at the surface level, 850 hPa, and 500 hPa, respectively. On January 13, BTH is on the north of a high pressure at the surface level, causing the southerly wind in/on the east of BTH, and sandwiched between the trough in the northeast of BTH and the high pressure in the southwest of BTH at 850 hPa, inducing the westerly surface wind in the west of BTH. At 500 hPa, the BTH is situated in the rear of the trough, and the westerly airflow is dominant. The air pollutants in BTH are subject to be transported to the east but hindered by the southerly wind, causing accumulation of air pollutants. On January 14, the high pressure system begins to control BTH at the surface level and 850 hPa, and the wind is varied and weak, favorable for the accumulation of air pollutants in BTH. On January 15, the BTH is still controlled by the high pressure at the surface level and 850 hPa, and the westerly wind is prevailing at the 500 hPa. The weak surface wind, together with the stable stratification, further facilitates accumulation of air pollutants in the BTH. On January 16, a trough develops over the BTH at 850 hPa and 500 hPa, and the BTH is situated near the trough line, in which the northerly and southerly wind occurs at the same time. At the surface level, the northerly wind is prevailing in the north of BTH and the southerly wind is prevalent in the south of BTH, leading to evacuation of air pollutants in the north of BTH and the high level of air pollutants in the south of BTH. On January 17, the trough at 850 hPa commences to weaken and the controlling region of the trough at 500 hPa becomes narrow. The northwesterly wind is dominant over BTH, leading to divergence of the air pollutants in BTH. On January 18, the BTH is located near the ridgeline at 850hPa and at the verge of the high pressure at the surface level. The controlling scope of high-pressure system on the surface level is wide,

inducing the varied wind over the BTH and is not conducive to the evacuation of air pollutants in BTH. On January 19, the prevailing southerly wind in the south of BTH and the strong westerly wind in the west of BTH lead to the convergence of air pollutants at the surface level. At 850 hPa and 500 hPa, BTH is situated in the southeast of the trough and southwesterly wind is prevalent. On January 20, the BTH is located in the southwest of the trough at 500 hPa and 850 hPa, and the strong northwesterly wind is prevailing over the BTH. At the surface level, the BTH is situated between the high pressure in the west and the low pressure in the east, inducing the strong northwesterly wind over BTH. The cold clean air sweeps BTH and efficiently decreases the air pollutant concentrations in BTH.

3.2 Uncertainties in Meteorological Simulations

Figures 4a-d provide the temporal profiles of the ensemble simulations of the surface meteorological fields and the corresponding observations at the meteorological site in Beijing from 13 to 20 January 2014. The U component exhibits larger ensemble spread than the V component (Figure s4), but the ensemble mean (ENSM) of the U component generally yields the observed diurnal variations. The ensemble prediction of the V component fails to reproduce the observed intensified southerly or northerly winds. The meteorological site is located on the north of the Yanshan Mountains, substantially influenced by the mountain-valley circulation (MVC). Apparently, the WRF-CHEM model lacks the ability to well simulate the occurrence and development of MVC, causing the considerable biases of the ensemble prediction of the V component. The ensemble prediction performs well in producing the diurnal variation of the surface temperature, but the underestimation or overestimation is still large when the V component prediction is biased. The relative humidity (RH) shows a rather large ensemble spread (Figure s4d), and the ENSM reasonably tracks the observed diurnal variation, with high nighttime and low afternoon simulated RH. The RH simulation is sensitive to the simulated surface temperature. Generally, the

overestimation of the surface temperature well corresponds to the underestimation of the RH, or vice versa. The ENSM considerably overestimates the PBL height during daytime on January 13 and 14, and underestimates on January 15 (Figure 4e). In addition, most of the ensemble members frequently underestimate the observed PBL height during nighttime, and all ensemble members fail to produce the peak PBL height on January 17 and 20. The PBL height is principally determined by the vertical shear of horizontal winds and the ground thermal condition. Therefore, uncertainties of wind and temperature field simulations cause large biases of the PBL height simulation.

3.3 Uncertainties in Aerosol Species Simulations

Figure 5 shows the temporal profiles of the ensemble simulations of the aerosol species and the observations at IRSDE in Beijing. The ENSM reasonably produces the observed variations of the POA concentrations. However, all ensemble members fail to capture the peaks in the morning on January 16 and in the evening on January 17, indicating that the underestimation might not be caused by the meteorological uncertainties, but by emission biases. The POA in the atmosphere is from multiple sources, including the direct emissions from vehicles, cooking, biomass and coal combustion. Diurnal variations of those sources might constitute one of the major reasons for the biases of the POA simulations. The ENSM generally performs reasonably well in simulating the SOA concentration against the measured OOA. The ratio of the ensemble spread to the ensemble mean (RESM) for the SOA prediction is large compared to that of POA (Figures s5a, b). Four SOA formation pathways are included in simulations: oxidations of anthropogenic and biogenic volatile organic compounds (VOCs), oxidation HOA semi-volatile vapors, and irreversible uptake of glyoxal and methylglyoxal on aerosol surfaces. Therefore, uncertainties in meteorological fields not only influence the transport of the SOA precursors but also the SOA formation processes in the atmosphere, causing the rather large RESM of SOA simulations. The ENSM generally

reproduces the observed variations of sulfate, nitrate and ammonium (SNA), but the RESM of SNA is also considerably large (Figures s5c-d). During haze days, sulfate is primarily formed through heterogeneous reactions of SO_2 on aerosol surfaces, which is highly dependent on the relative humidity (Li et al., 2017). Nitrate formation is determined by the HNO_3 and N_2O_5 originated from the NO_2 oxidation, sensitive to the temperature and relative humidity and also influenced by the level of sulfate in the particle phase and ammonia in the atmosphere. The ammonium aerosol is formed through neutralization of sulfate and nitrate aerosols by NH_3 . Additionally, in the present study, ISORROPIA (Version 1.7) is used to calculate the thermodynamic equilibrium between the sulfate-nitrate-ammonium-water aerosols and their gas phase precursors H_2SO_4 - HNO_3 - NH_3 -water vapor. Therefore, uncertainties of meteorological fields propagate to the transport, atmospheric oxidation, and thermal dynamic processes, which all have contributions to the large RESM of the SNA simulations. Apparently, uncertainties in meteorological conditions substantially affect the aerosol species simulations at a single observation site, which is consistent with the previous studies (Bei et al., 2012).

3.4 Uncertainties in $\text{PM}_{2.5}$ Simulations in BTH

Heavy haze with high levels of $\text{PM}_{2.5}$ frequently constitutes a regional pollution event. Figure 6 shows the temporal profiles of the ensemble simulations and observations of air pollutants averaged at the monitoring sites in BTH from 13 to 20 January 2014. The RESM of the average air pollutants is much less than those of aerosol species at the single observation site (Figure s6). For the primary air pollutants, SO_2 and CO, the ENSM generally tracks reasonably the observed variations. However, sometimes all the ensemble members underestimate or overestimate the observation. There are two possible reasons for the biases of ensemble simulations of SO_2 and CO: uncertainties of emissions and systematic errors of meteorological fields. In the evening on January 15, the ensemble prediction substantially

overestimates the observed SO₂ concentration, but CO overestimation is not large. In the contrast, in the morning on January 16, the ensemble prediction slightly underestimates the SO₂ observation but remarkably underestimates the CO concentration. Therefore, the overestimation of SO₂ on January 15 and underestimation of CO on January 16 might be primarily contributed by the emission uncertainties. In the morning on January 18, the ensemble prediction significantly underestimates both SO₂ and CO observations, indicating the plausible uncertainties caused by the systematic errors of meteorological fields.

The ENSM of the average surface O₃ and NO₂ over the monitoring sites in BTH is in good agreement with observations. The ensemble prediction is subject to underestimate the O₃ observation during nighttime, but well consistent with the NO₂ observation. Considering the massive NO_x emission and the titration of NO, the nighttime O₃ concentrations are generally very low, particularly during wintertime when the daytime O₃ concentrations are not high. Hence, the underestimation of nighttime O₃ concentrations is perhaps caused by the observation uncertainties, such as the setting of lower detection limit. In addition, the ENSM does not reproduce the high O₃ level during nighttime on January 19 when the northwesterly wind is intensified to evacuate the air pollutants in BTH. Rapid increase of the observed O₃ concentrations during nighttime shows the substantial contribution of the background O₃ transport. Therefore, the background O₃ uncertainties constitute the major reason for the O₃ underestimation on January 19.

The ENSM also performs well in replicating the observed PM_{2.5} observation, except the underestimation on January 16 and 18. However, the RESM of the PM_{2.5} simulations is larger than those of O₃, NO₂, SO₂, and CO (Figure s6). The average ENSM of the PM_{2.5} concentration over the monitoring sites during the simulation period is 189.5 µg m⁻³, close to the observed 197.6 µg m⁻³. In addition, the ensemble member of 16 and 30 (EN-16 and EN-30, respectively) produces the highest and lowest PM_{2.5} level, with the average PM_{2.5}

concentrations of 231.5 and 167.3 $\mu\text{g m}^{-3}$, respectively. The $\text{PM}_{2.5}$ mainly include the primary aerosols which are determined by direct emissions, and the secondary aerosols which are determined by their precursors emissions and the homogeneous and heterogeneous oxidation process in the atmosphere. Therefore, the large RESM of SOA and SNA simulations enhances the ensemble spread of the $\text{PM}_{2.5}$ simulations.

Figure 7 presents the spatial distributions of ENSM and observations of the daily average near-surface $\text{PM}_{2.5}$ mass concentrations during the haze episode, along with the simulated wind fields. The ENSM predicted $\text{PM}_{2.5}$ spatial patterns are generally in good agreement with the observations at the ambient monitoring sites in BTH. The ENSM successfully reproduces the haze development and maturity stages from January 13 to 16, 2014. From January 17 to 18, the northeasterly wind develops and decreases the $\text{PM}_{2.5}$ level in BTH, but not strong enough to evacuate the air pollutants. The $\text{PM}_{2.5}$ pattern of ENSM is well consistent with observations, but on January 18, the $\text{PM}_{2.5}$ concentrations are remarkably underestimated in four cities in BTH. On January 19, the westerly wind is prevailing in BTH, causing the divergence of the $\text{PM}_{2.5}$. On January 20, the intensified northwesterly wind commences to empty the $\text{PM}_{2.5}$ in BTH. However, apparently, the occurrence of the intensification of the northwesterly wind is early, causing considerable underestimation of the $\text{PM}_{2.5}$ concentration in the ENSM.

The uncertainties in meteorological fields are generally less than observational and analysis errors, but the ensemble simulations still exhibit considerable spreads. In order to contrast the $\text{PM}_{2.5}$ simulations of different ensemble members, we have selected two members: EN-16 and EN-30, representing the highest and lowest $\text{PM}_{2.5}$ simulations in BTH, respectively. Figure 8 provides the horizontal distributions of the daily average surface $\text{PM}_{2.5}$ concentrations along with surface winds during the episode in EN-16 and EN-30. Similar $\text{PM}_{2.5}$ distribution patterns are simulated in EN-16 and EN-30, showing that the

meteorological uncertainties do not dominate the haze formation and development principally. The $PM_{2.5}$ level in EN-16 is much higher than that in EN-30 in BTH, which is mainly caused by the considerable discrepancies in the surface winds between the two members. The simulated southerly wind in EN-16 is generally more intense than that in EN-30, but the northerly wind in EN-16 is weak compared to EN-30, which is more favorable for the air pollutants accumulation in EN-16 than EN-30. On January 13 and 14, the winds in EN-30 are weak or calm in BTH and the $PM_{2.5}$ is mainly attributed to the local production. However, in EN-16, the prevailing south winds also deliver the air pollutants from the south areas to BTH, substantially enhancing the $PM_{2.5}$ level. On January 15, although EN-16 and EN-30 both produce the prevailing southerly wind in BTH, the westerly wind in EN-30 is intense compared to EN-16, considerably decreasing the $PM_{2.5}$ level in EN-30. On January 16, the northeasterly wind in EN-30 is intensified and evacuates the $PM_{2.5}$ in the north of BTH. However, in EN-16, the simulated northeasterly wind is weak and the $PM_{2.5}$ level in the north of BTH still remains high. On January 17, the simulated northerly wind in EN-16 is weak compared to that in EN-30, causing higher $PM_{2.5}$ concentration in EN-16 than EN-30 in BTH. On January 18, the intensified southerly wind in EN-16 considerably increases the $PM_{2.5}$ level in BTH compared to EN-30. On January 19, the westerly wind is prevalent in EN-30 and the $PM_{2.5}$ level commences to decrease, but in EN-16, the southwesterly wind still causes high $PM_{2.5}$ concentrations in BTH. On January 20, the stronger northeasterly wind in EN-30 more efficiently evacuates the $PM_{2.5}$ than that in EN-16.

3.5 Uncertainties in $PM_{2.5}$ Simulations in Mega-cities

EN-16 and EN-30 both predict the haze occurrence and development in BTH during the episode, although the difference of the $PM_{2.5}$ level between those two members is considerable, showing that the meteorological uncertainties do not dominate the regional haze formation. Previous studies have shown that the meteorological uncertainties

substantially impact the air quality simulations at the city-scale (Bei et al., 2012). Figure 10 presents the temporal variation of the ensemble simulations and observations averaged at four mega-cities in BTH during the episode. The ENSM of the $PM_{2.5}$ concentrations in Beijing, Tianjin, and Baoding is in good agreement with the observation. However, the ENSM remarkably underestimates the observed $PM_{2.5}$ concentration in Shijiazhuang from January 16 to 19, which is hardly interpreted by the emission biases. The ENSM performs well in simulating the $PM_{2.5}$ variations from January 13 to 15, and overestimates the observation on January 20 in Shijiazhuang. One of the possible reasons for the underestimation in Shijiazhuang is that the westerly wind is systematically overestimated from January 16 to 19 along the foothills of the Taihang Mountains, causing the haze plume to move eastwardly.

Although the ENSM produces reasonably well the $PM_{2.5}$ variations in the four mega-cities against the measurement, the meteorological uncertainties still cause large uncertainties of the $PM_{2.5}$ concentration (Figure s7). During the first three days of the episode, the ENSM is well consistent with the observations in the four mega-cities, but the $PM_{2.5}$ level discrepancy between the members with the highest and lowest $PM_{2.5}$ concentrations is rather large, causing troubles for the **assessment** of the control strategies. For example, in Shijiazhuang, the average $PM_{2.5}$ concentrations during the first three days in the members with the highest and lowest $PM_{2.5}$ concentrations are 403.5 and 213.8 $\mu g m^{-3}$, respectively, and the difference is about 190 $\mu g m^{-3}$. In Beijing, the average $PM_{2.5}$ concentrations in the two members are 103.9 and 196.3 $\mu g m^{-3}$. It is worth noting that, according to the Chinese air quality standard released in 2012, the $PM_{2.5}$ concentration of 103.9 $\mu g m^{-3}$ is defined as “lightly polluted condition”, but 196.3 $\mu g m^{-3}$ defined as “heavily polluted condition”. If the heavy air pollution occurs, the control strategies will be implemented. Therefore, it is necessary to use the ensemble simulation to avoid the impact of the meteorological uncertainties on the haze prediction.

4 Summary and Conclusions

In the present study, the uncertainties in simulating haze formation due to meteorological uncertainties are investigated using the WRF-CHEM model through ensemble simulations. A persistent heavy haze episode occurred in BTH from 13 to 20 is simulated. A climatological ensemble initialization approach is used to produce initial and boundary conditions for each ensemble member.

The ENSMs of the aerosol constituents are generally in good agreement with the observations at an observation site in Beijing, including the sharp buildup of the aerosol constituents in the evening on January 15 and rapid falloff in the morning on January 20. However, the ENSM considerably underestimates the observed primary aerosols in the evening on January 17. The ensemble spread is rather large for the aerosol constituent simulations, and the RESM exceeds 50%, respectively.

The ENSM performs well in simulating the temporal variations of the average surface CO, SO₂, NO₂, O₃ and PM_{2.5} mass concentrations over the monitoring sites in BTH, and the RESM of the air pollutants is generally less than 30%. The RESM of PM_{2.5} simulations is larger than the other air pollutants, which is due to the complicated composition of PM_{2.5}, including the contributions of primary and secondary aerosols. The meteorological uncertainties do not principally dominate the haze formation and development, but considerably alter the simulated PM_{2.5} level. The average PM_{2.5} difference during the episode exceeds 60 $\mu\text{g m}^{-3}$ between the two members with the highest and lowest PM_{2.5} simulations.

Although the meteorological uncertainties do not dominate the regional haze formation, they still substantially influence the PM_{2.5} simulations at city-scale. The ENSM reasonably well predicts the PM_{2.5} variations in the four mega-cities against the measurements, including Beijing, Tianjin, Baoding and Shijiazhuang, but the RESM of the PM_{2.5} simulations is rather

large, causing troubles for the evaluation of the control strategies. Therefore, the ensemble simulation is needed to take into consideration the impact of the meteorological uncertainties on the haze prediction. It is worth noting that aside from meteorological fields, uncertainties in emissions or various chemistry/aerosol schemes also considerably influence the WRF-CHEM model simulations. The extended response surface modeling (ERSM) technique can be used to quantify the relative importance of each uncertainty source in the WRF-CHEM model (Zhao et al, 2017).

Acknowledgement: Naifang Bei is supported by the National Natural Science Foundation of China (no. 41275101 and no. 41430424) and the Fundamental Research Funds for the Central Universities of China. Guohui Li is supported by “Hundred Talents Program” of the Chinese Academy of Sciences and the National Natural Science Foundation of China (no. 41661144020). This work is financially supported by National Key R&D Plan (Quantitative Relationship and Regulation Principle between Regional Oxidation Capacity of Atmospheric and Air Quality (2017YFC0210000)).

References

- Beekmann, M. and Derognat, C.: Monte Carlo uncertainty analysis of a regional-scale chemistry model constrained by measurements from the Atmospheric Pollution Over the Paris Area (ESQUIF) campaign, *J. Geophys. Res.*, 108, 8559, doi:10.1029/2003JD003391, 2003.
- Bei, N., de Foy, B., Lei, W., Zavala, M., and Molina, L. T.: Using 3DVAR data assimilation system to improve ozone simulations in the Mexico City basin, *Atmos. Chem. Phys.*, 8, 7353–7366, 2008.
- Bei, N., Lei, W., Zavala, M., and Molina, L. T.: Ozone predictabilities due to meteorological uncertainties in the Mexico City basin using ensemble forecasts, *Atmos. Chem. Phys.*, 10, 6295–6309, doi:10.5194/acp-10-6295-2010, 2010.
- Bei, N., Li, G., and Molina, L. T.: Uncertainties in SOA simulations due to meteorological uncertainties in Mexico City during MILAGRO-2006 field campaign, *Atmos. Chem. Phys.*, 12, 11295–11308, doi:10.5194/acp-12-11295-2012, 2012.
- Bei, N., Li, G., Huang, R., Cao, J., Meng, N., Feng, T., Liu, S., Zhang, T., Zhang, Q., and Molina, L. T.: Typical synoptic situations and their impacts on the wintertime air pollution in the Guanzhong basin, China, *Atmos. Chem. Phys.*, 16, 7373–7387, 2016a.
- Bei, N., Xiao, B., Meng, N., and Feng, T.: Critical role of meteorological conditions in a persistent haze episode in the Guanzhong basin, China, *Sci. Total Environ.*, 550, 273–284, 2016b.
- Binkowski, F. S. and Roselle, S. J.: Models-3 Community Multiscale Air Quality (CMAQ) model aerosol component: 1. Model description, *J. Geophys. Res.*, 108, 4183, doi:10.1029/2001JD001409, 2003.
- Chan, C. K., and Yao, X.: Air pollution in mega cities in China, *Atmos. Environ.*, 42, 1–42, 2008.
- Chen, F., and Dudhia, J.: Coupling an advanced land surface-hydrology model with the Penn State-NCAR MM5 modeling system. Part I: Model implementation and sensitivity, *Mon. Weather Rev.*, 129, 569–585, 10.1175/1520-0493(2001) 129<0569:caalsh>2.0.co; 2, 2001.
- Chou, M. D., and Suarez, M. J.: A solar radiation parameterization for atmospheric studies, NASA TM-104606, Nasa Tech.memo, 15, 1999.
- Chou, M. D., Suarez, M. J., Liang, X. Z., Yan, M. H., and Cote, C.: A Thermal Infrared Radiation Parameterization for Atmospheric Studies, Max J, 2001.
- Canonaco, F., Crippa, M., Slowik, J. G., Baltensperger, U., and Prevot, A. S. H.: SoFi, an IGOR-based interface for the efficient use of the generalized multilinear engine (ME-2) for the source apportionment: ME-2 application to aerosol mass spectrometer data, *Atmos. Meas. Tech.*, 6(12), 3649–3661, 2013.
- Delle Monache, L. and Stull, R.: An ensemble air quality forecast over western Europe during an ozone forecast, *Atmos. Environ.*, 37, 3469–3474, 2003.
- Delle Monache, L., Deng, X., Zhou, Y., and Stull, R.: Ozone ensemble forecasts: A new ensemble design, *J. Geophys. Res.*, 111, D05307, doi:10.1029/2005JD006310, 2006.
- Dabberdt, W. F., Carroll, M. A., Baumgardner, D., Carmichael, G., Cohen, R., Dye, T., Ellis, J., Grell, G., Grimmond, S., Hanna, S., Irwin, J., Lamb, B., Madronich, S., Mcqueen, J., Meagher, J., Odman, T., Pleim, J., Schmid, H. P., and Westphal, D. L.: Meteorological research needs for improved air quality forecasting: Report of the 11th Prospectus

450 Development Team of the U.S. Weather Research Program, *B. Am. Meteorol. Soc.*, 85,
451 563–586, 2004.

452 Dabberdt, W. F. and Miller E.: Uncertainty, ensembles and air quality dispersion modeling:
453 Applications and challenges, *Atmos. Environ.*, 34, 4667–4673, 2000.

454 Elser, M., Huang, R.-J., Wolf, R., Slowik, J. G., Wang, Q., Canonaco, F., Li, G., Bozzetti, C.,
455 Daellenbach, K. R., Huang, Y., Zhang, R., Li, Z., Cao, J., Baltensperger, U., El-Haddad,
456 I., and Prévôt, A. S. H.: New insights into PM_{2.5} chemical composition and sources in two
457 major cities in China during extreme haze events using aerosol mass spectrometry, *Atmos.*
458 *Chem. Phys.*, 16, 3207–3225, <https://doi.org/10.5194/acp-16-3207-2016>, 2016

459 Fang, M., Chan, C. K., and Yao, X. H.: Managing air quality in a rapidly developing nation:
460 China, *Atmos. Environ.*, 43, 79–86, 2009.

461 Feng, T., Li, G., Cao, J., Bei, N., Shen, Z., Zhou, W., Liu, S., Zhang, T., Wang, Y., Huang,
462 R.-J., Tie, X., and Molina, L. T.: Simulations of organic aerosol concentrations during
463 springtime in the Guanzhong Basin, China, *Atmos. Chem. Phys.*, 16, 10045–10061,
464 <https://doi.org/10.5194/acp-16-10045-2016>, 2016.

465 Galmarini, S., Bianconi, R., Klug, W., Mikkelsen, T., Addis, R., An- dronopoulos, S., Astrup,
466 P., Baklanov, A., Bartniki, J., Bartzis, J. C., Bellasio, R., Bompay, F., Buckley, R.,
467 Bouzom, M., Champion, H., D’Amours, R., Davakis, E., Eleveld, H., Geertsema, G. T.,
468 Glaab, H., Kollax, M., Ilvonen, M., Manning, A., Pechinger, U., Persson, C., Polreich, E.,
469 Potemski, S., Prodanova, M., Salt- bones, J., Slaper, H., Sofiev, M. A., Syrakov, D.,
470 Sørensen, J. H., Van der Auwera, L., Valkama, I., and Zelazny, R.: Ensemble dispersion
471 forecasting – Part I: Concept, approach and indicators, *Atmos. Environ.*, 38, 4607–4617,
472 2004.

473 Gao, Y., Liu, X., Zhao, C., and Zhang, M.: Emission controls versus meteorological
474 conditions in determining aerosol concentrations in Beijing during the 2008 Olympic
475 Games, *Atmos. Chem. Phys.*, 11, 12437–12451, [doi:10.5194/acp-11-12437-2011](https://doi.org/10.5194/acp-11-12437-2011), 2011.

476 Guenther, A., Karl, T., Harley, P., Wiedinmyer, C., Palmer, P. I., and Geron, C.: Estimates of
477 global terrestrial isoprene emissions using MEGAN (Model of Emissions of Gases and
478 Aerosols from Nature), *Atmos. Chem. Phys.*, 6, 3181–3210, [doi:10.5194/acp-6-3181-](https://doi.org/10.5194/acp-6-3181-2006)
479 2006, 2006.

480 Guo, S., M. Hu, M. L. Zamora, J. Peng, D. Shang, J. Zheng, Z. Du, Z. Wu, M. Shao, L. Zeng,
481 M. J. Molina, and R. Zhang: Elucidating severe urban haze formation in China, *P. Natl.*
482 *Acad. Sci. USA*, 111, 17373–17378, 2014.

483 Hong, S.-Y., Dudhia, J., and Chen, S.-H.: A revised approach to ice microphysical processes
484 for the bulk parameterization of clouds and precipitation, *Mon. Wea. Rev.*, 132, 103–120,
485 2004.

486 Horowitz, L. W., Waters, S., Mauzerall, D. L., Emmons, L. K., Rasch, P. J., Tie, X.,
487 Lamarque, J.-F., Schultz, M. G., Tyndall, G. S., Orlando, J. J., and Brasseur, G. P.: A
488 global simulation of tropospheric ozone and related tracers: Description and evaluation of
489 MOZART, version 2, *J. Geophys. Res.*, 108, 4784, [doi:10.1029/2002JD002853](https://doi.org/10.1029/2002JD002853), 2003.

490 Huang, R. J., Zhang, Y. L., Bozzetti, C., Ho, K. F., Cao, J. J., Han, Y. M., Dällenbach, K. R.,
491 Slowik, J. G., Platt, S. M., Canonaco, F., Zotter, P., Wolf, R., Pieber, S. M., Bruns, E. A.,
492 Crippa, M., Ciarelli, G., Piazzalunga, A., Schwikowski, M., Abbaszade, G., Schnelle-
493 Kreis, J., Zimmermann, R., An, Z. S., Szidat, S., Baltensperger, U., El Haddad, I., Prévôt,

494 A. S. H.: High secondary aerosol contribution to particulate pollution during haze events
 495 in China, *Nature*, 514, 218–222, 2014.

496 Janjic, Z. I.: Nonsingular implementation of the Mellor-Yamada level 2.5 scheme in the
 497 NCEP Meso Model, NCEP Office Note, 437, 61 pp., 2002.

498 Li, G., Lei, W., Zavala, M., Volkamer, R., Dusanter, S., Stevens, P., Molina, L.T.: Impacts of
 499 HONO sources on the photochemistry in Mexico City during the MCMA-2006/MILAGO
 500 Campaign, *Atmos. Chem. Phys.*, 10, 6551–6567, 2010.

501 Li, G., Bei, N., Tie, X., and Molina, L. T.: Aerosol effects on the photochemistry in Mexico
 502 City during MCMA-2006/MILAGRO campaign, *Atmos. Chem. Phys.*, 11, 5169–5182,
 503 10.5194/acp-11-5169-2011, 2011a.

504 Li, G., Zavala, M., Lei, W., Tsimpidi, A. P., Karydis, V. A., Pandis, S. N., Canagaratna, M.
 505 R., and Molina, L. T.: Simulations of organic aerosol concentrations in Mexico City using
 506 the WRF-CHEM model during the MCMA-2006/MILAGRO campaign, *Atmos. Chem.*
 507 *Phys.*, 11, 3789–3809, 10.5194/acp-11-3789-2011, 2011b.

508 Li, G., Lei, W., Bei, N., and Molina, L. T.: Contribution of garbage burning to chloride and
 509 PM_{2.5} in Mexico City, *Atmos. Chem. Phys.*, 12, 8751–8761, 10.5194/acp-12-8751-2012,
 510 2012.

511 Li, G., Bei, N., Cao, J., Huang, R., Wu, J., Feng, T., Wang, Y., Liu, S., Zhang, Q., and Tie, X.:
 512 A possible pathway for rapid growth of sulfate during haze days in China, *Atmos. Chem.*
 513 *Phys.*, 17, 1-43, 2017.

514 Li, G., Bei, N., Cao, J., Wu, J., Long, X., Feng, T., Dai, W., Liu, S., Zhang, Q., and Tie, X.:
 515 Widespread and persistent ozone pollution in eastern China during the non-winter season
 516 of 2015: observations and source attributions, *Atmos. Chem. Phys.*, 17, 2759–2774,
 517 doi:10.5194/acp-17-2759-2017, 2017.

518 Liu, T., Gong, S., He, J., Yu, et al.: Attributions of meteorological and emission factors to the
 519 2015 winter severe haze pollution episodes in China's Jing-Jin-Ji area, *Atmos. Chem.*
 520 *Phys.*, 17, 2971–2980, doi:10.5194/acp-17-2971-2017, 2017.

521 Mallet, V. and Sportisse, B.: Ensemble-based air quality forecasts: A multi-model approach
 522 applied to ozone, *J. Geophys. Res.*, 111, D18302, doi:10.1029/2005JD006675, 2006.

523 Menut, L.: Adjoint modeling for atmospheric pollution process sensitivity at regional scale, *J.*
 524 *Geophys. Res.*, 108, 8562, doi:10.1029/2002JD002549, 2003.

525 McKeen, S., Wilczak, J., Grell, G., Djalalova, I., Peckham, S., Hsie, E.-Y., Gong, W.,
 526 Bouchet, V., Menard, S., Moffet, R., McHenry, J., McQueen, J., Tang, Y., Carmichael, G.
 527 R., Pagowski, M., Chan, A., Dye, T., Frost, G., Lee, P., and Mathur, R.: Assessment of an
 528 ensemble of seven realtime ozone forecasts over eastern North America during the
 529 summer of 2004, *J. Geophys. Res.*, 110, D21307, doi:10.1029/2005JD005858, 2005.

530 Nenes, A., Pandis, S. N., and Pilinis, C.: ISORROPIA: A new thermodynamic equilibrium
 531 model for multiphase multicomponent inorganic aerosols, *Aquat. Geochem.*, 4, 123–152,
 532 10.1023/a:1009604003981, 1998.

533 Penner, J. E. et al. Aerosols, their direct and indirect effects, in: *Climate Change 2001: The*
 534 *Scientific Basis*, Contributions of Working Group I to the Third Assessment Report of the
 535 Intergovernmental Panel on Climate Change, edited by: Houghton, J. T., Ding, Y., Griggs,
 536 D. J., Noguer, M., van der Linden, P. J., Dai, X., Maskell K., and Johnson, C. A.,
 537 Cambridge University Press, Cambridge, UK, and New York, NY, USA, 289–348, 2001.

538 Pope III, C. A. and Dockery, D. W.: Health effects of fine particulate air pollution: Liens that
539 connect, *J. Air. Waste Manage*, 56, 709–742, 2006.

540 Sharma, A., Ojha, N., Pozzer, A., Mar, K. A., Beig, G., Lelieveld, J., and Gunthe, S., WRF-
541 Chem simulated surface ozone over South Asia during the pre-monsoon: Effects of
542 emission inventories and chemical mechanisms, *Atmos. Chem. Phys. Discuss.*,
543 doi:10.5194/acp-2016-1083, in review, 2016.

544 Nielsen-Gammon, J. W., McNider, R. T., Angevine, W. M., White, A. B., and Knupp, K.:
545 Mesoscale model performance with assimilation of wind profiler data: Sensitivity to
546 assimilation parameters and network configuration. *J. Geophys. Res.*, 112, D09119,
547 doi:10.1029/2006JD007633, 2007.

548 Solazzo, E., Bianconi, R., Hogrefe, C., Curci, G., Tuccella, P., Alyuz, U., Balzarini, A., Baró,
549 R., Bellasio, R., Bieser, J., Brandt, J., Christensen, J. H., Colette, A., Francis, X., Fraser,
550 A., Vivanco, M. G., Jiménez-Guerrero, P., Im, U., Manders, A., Nopmongkol, U.,
551 Kitwiroon, N., Pirovano, G., Pozzoli, L., Prank, M., Sokhi, R. S., Unal, A., Yarwood, G.,
552 and Galmarini, S.: Evaluation and error apportionment of an ensemble of atmospheric
553 chemistry transport modeling systems: multivariable temporal and spatial breakdown,
554 *Atmos. Chem. Phys.*, 17, 3001–3054, <https://doi.org/10.5194/acp-17-3001-2017>, 2017.

555 Wang, H., Xu, J., Zhang, M., Yang, Y., Shen, X., Wang, Y., Chen, D., Guo, J.: A study of the
556 meteorological causes of a prolonged and severe haze episode in January 2013 over
557 central-eastern China, *Atmos. Environ.*, 98, 146–157, 2014.

558 Williams, L. R., Gonzalez, L. A., Peck, J., Trimborn, D., McInnis, J., Farrar, M. R., Moore, K.
559 D., Jayne, J. T., Robinson, W. A., Lewis, D. K., Onasch, T. B., Canagaratna, M. R.,
560 Trimborn, A., Timko, M. T., Magoon, G., Deng, R., Tang, D., Blanco, E., Prevot, A. S.
561 H., Smith, K. A., and Worsnop, D. R.: Characterization of an aerodynamic lens for
562 transmitting particles greater than 1 micrometer in diameter into the Aerodyne aerosol
563 mass spectrometer, *Atmos. Meas. Tech.*, 6(11), 3271–3280, 2013.

564 Wu, J., Li, G., Cao, J., Bei, N., Wang, Y., Feng, T., Huang, R., Liu, S., Zhang, Q., and Tie, X.:
565 Contributions of trans-boundary transport to summertime air quality in Beijing, China,
566 *Atmos. Chem. Phys.*, 17, 2035–2051, doi:10.5194/acp-17-2035-2017, 2017.

567 Wu, M., Wu, D., Fan, Q., Wang, B. M., Li, H. W., and Fan, S. J.: Observational studies of the
568 meteorological characteristics associated with poor air quality over the Pearl River Delta
569 in China, *Atmos. Chem. Phys.*, 13, 10755–10766, doi:10.5194/acp-13-10755-2013, 2013.

570 Zhang, F., Bei, N., Nielsen-Gammon, J. W., Li, G., Zhang, R., Stuart, A. L., and Aksoy, A.:
571 Impacts of meteorological uncertainties on ozone pollution predictability estimated
572 through meteorological and photochemical ensemble forecasts, *J. Geophys. Res.*, 112,
573 D04304, doi:10.1029/2006JD007429, 2007.

574 Zhang, J. P., Zhu, T., Zhang, Q. H., Li, C. C., Shu, H. L., Ying, Y., Dai, Z. P., Wang, X., Liu,
575 X. Y., Liang, A. M., Shen, H. X., and Yi, B. Q.: Impact of circulation patterns on
576 transport paths and air quality, *Atmos. Chem. Phys.*, 12, 5031–5053, 2012.

577 Zhang, Q., Streets, D. G., Carmichael, G. R., He, K. B., Huo, H., Kannari, A., Klimont, Z.,
578 Park, I. S., Reddy, S., Fu, J. S., Chen, D., Duan, L., Lei, Y., Wang, L. T., and Yao, Z. L.:
579 Asian emissions in 2006 for the NASA INTEX-B mission, *Atmos. Chem. Phys.*, 9, 5131–
580 5153, 2009.

581 Zhang, Q., Quan, J., Tie, X., Li, X., Liu, Q., Gao, Y., and Zhao, D.: Effects of meteorology
582 and secondary particle formation on visibility during heavy haze events in Beijing, China,
583 *Sci. Total Environ.*, 502, 578–584, 2015.

584 Zhang, R., Li, G., Fan, J., Wu, D. L., and Molina, M. J.: Intensification of Pacific storm track
585 linked to Asian pollution, *P. Natl. Acad. Sci. USA*, 104, 5295–5299, 2007.

586 Zhao, B., Wu, W., Wang, S., Xing, J., Chang, X., Liou, K.-N., Jiang, J. H., Gu, Y., Jang, C.,
587 Fu, J. S., Zhu, Y., Wang, J., Lin, Y., and Hao, J.: A modeling study of the nonlinear
588 response of fine particles to air pollutant emissions in the Beijing–Tianjin–Hebei region,
589 *Atmos. Chem. Phys.*, 17, 12031–12050, <https://doi.org/10.5194/acp-17-12031-2017>, 2017.

590 Zhao, X. J., Zhao, P. S., Xu, J., Meng, W., Pu, W. W., Dong, F., He, D., and Shi, Q. F.:
591 Analysis of a winter regional haze event and its formation mechanism in the North China
592 Plain, *Atmos. Chem. Phys.*, 13, 5685–5696, 2013.

593

594

Figure Captions

- Figure 1 WRF-CHEM simulation domain. The filled red (in BTH) and blue (outside of BTH) circles represent centers of cities with ambient monitoring site. The size of the circle denotes the number of ambient monitoring sites of cities. The filled black triangle and rectangle denote the deployment location of the HR-ToF-AMS and the surface meteorological site in Beijing, respectively.
- Figure 2 Vertical distribution of the mean of initial ensemble spreads and the standard deviation for (a) horizontal winds (U and V components), (b) temperature, (c) pressure, and (d) water vapor mixing ratio.
- Figure 3 Observed hourly $PM_{2.5}$ concentrations averaged in (a) four megacities (including Beijing, Tianjin, Baoding, and Shijiazhuang) and (b) nine non-megacities of BTH during the period from January 13 to 20, 2014.
- Figure 4 Temporal evolution of the surface (a) U component, (b) V component, (c) temperature, and (d) relative humidity at the meteorological site, and (e) the PBL height at IRSDE in Beijing from each ensemble member (thin green lines), the ensemble mean (bold black line), and observations (black dots) from January 13 to 20, 2014.
- Figure 5 Temporal evolution of the (a) POA, (b) SOA, (c) sulfate, (d) nitrate, and (e) ammonium mass concentrations at IRSDE in Beijing from each ensemble member (thin green lines), the ensemble mean (bold black line), and observations (black dots) from January 13 to 20, 2014.
- Figure 6 Temporal evolution of the (a) $PM_{2.5}$, (b) O_3 , (c) NO_2 , (d) SO_2 , and (e) CO mass concentrations averaged over monitoring sites in BTH from each ensemble member (thin green lines), the ensemble mean (bold black line), and observations (black dots) from January 13 to 20, 2014.
- Figure 7 ENSM of the daily average surface $PM_{2.5}$ concentration distributions (color contour) along with the ENSM of the daily average surface winds (black arrows) from January 13 to 20, 2014. The colored circles denote the $PM_{2.5}$ measurements in cities.
- Figure 8 Same as Figure 7, but for the ensemble member of 16 with the highest simulated $PM_{2.5}$ concentration.
- Figure 9 Same as Figure 7, but for the ensemble member of 30 with the lowest simulated $PM_{2.5}$ concentration.
- Figure 10 Temporal evolution of the $PM_{2.5}$ mass concentrations averaged in (a) Beijing, (b) Tianjin, (c) Baoding, and (d) Shijiazhuang from each ensemble member (thin green lines), the ensemble mean (bold black line), and observations (black dots) during the period from January 13 to 20, 2014. The red and blue lines represent the simulations in the members with highest and lowest $PM_{2.5}$ concentrations, respectively.

638 Table 1 WRF-CHEM model configurations
639

Regions	Beijing-Tianjin-Hebei (BTH)
Simulation period	January 13 to 21, 2014
Domain size	200 × 200
Domain center	39°N, 117°E
Horizontal resolution	6km × 6km
Vertical resolution	35 vertical levels with a stretched vertical grid with spacing ranging from 30 m near the surface, to 500 m at 2.5 km and 1 km above 14 km
Microphysics scheme	WSM 6-class graupel scheme (Hong and Lim, 2006)
Boundary layer scheme	MYJ TKE scheme (Janjić, 2002)
Surface layer scheme	MYJ surface scheme (Janjić, 2002)
Land-surface scheme	Unified Noah land-surface model (Chen and Dudhia, 2001)
Longwave radiation scheme	Goddard longwave scheme (Chou and Suarez, 2001)
Shortwave radiation scheme	Goddard shortwave scheme (Chou and Suarez, 1999)
Meteorological boundary and initial conditions	NCEP 1°×1° reanalysis data
Chemical initial and boundary conditions	MOZART 6-hour output (Horowitz et al., 2003)
Anthropogenic emission inventory	Developed by Zhang et al. (2009)
Biogenic emission inventory	MEGAN model developed by Guenther et al. (2006)

640
641
642
643
644

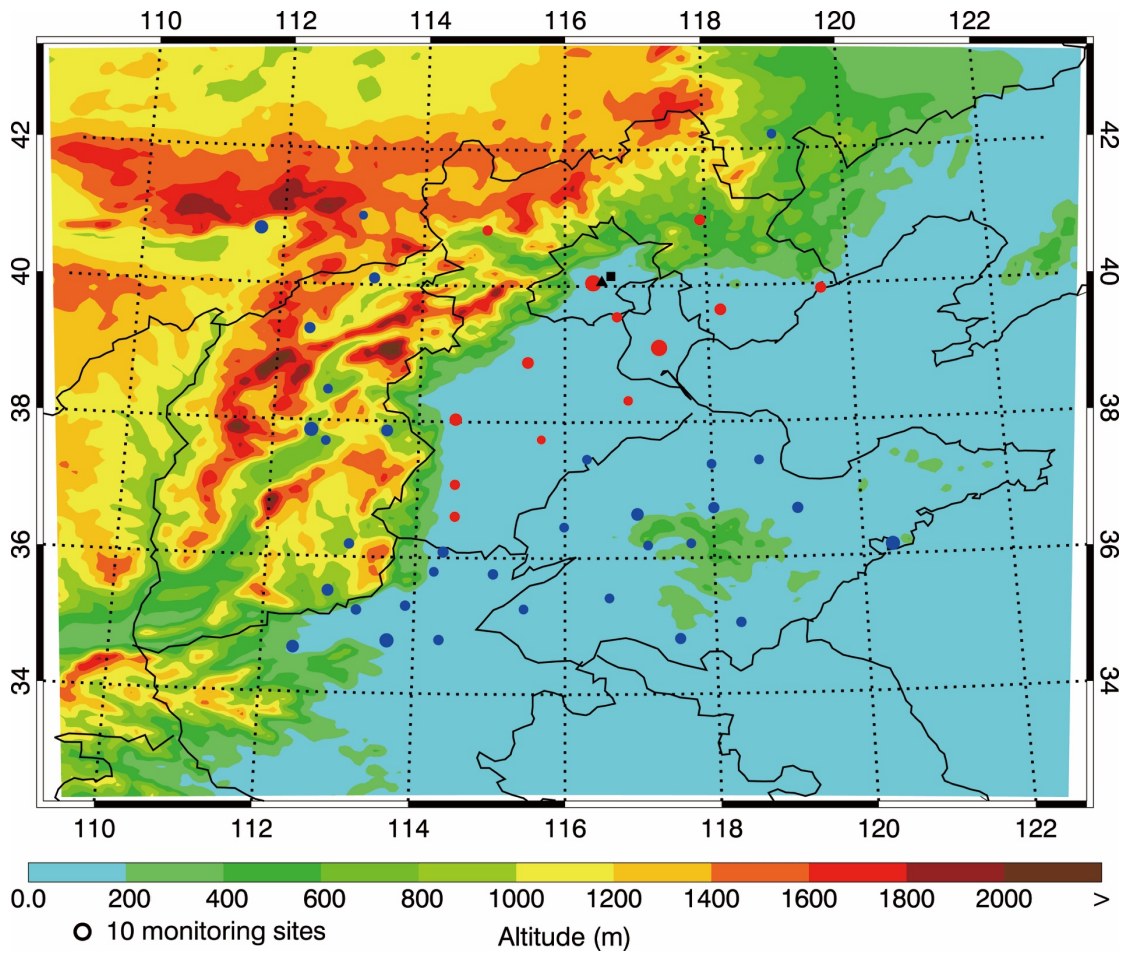


Figure 1 WRF-CHEM simulation domain. The filled red (in BTH) and blue (outside of BTH) circles represent centers of cities with ambient monitoring site. The size of the circle denotes the number of ambient monitoring sites of cities. The filled black triangle and rectangle denote the deployment location of the HR-ToF-AMS and the surface meteorological site in Beijing, respectively.

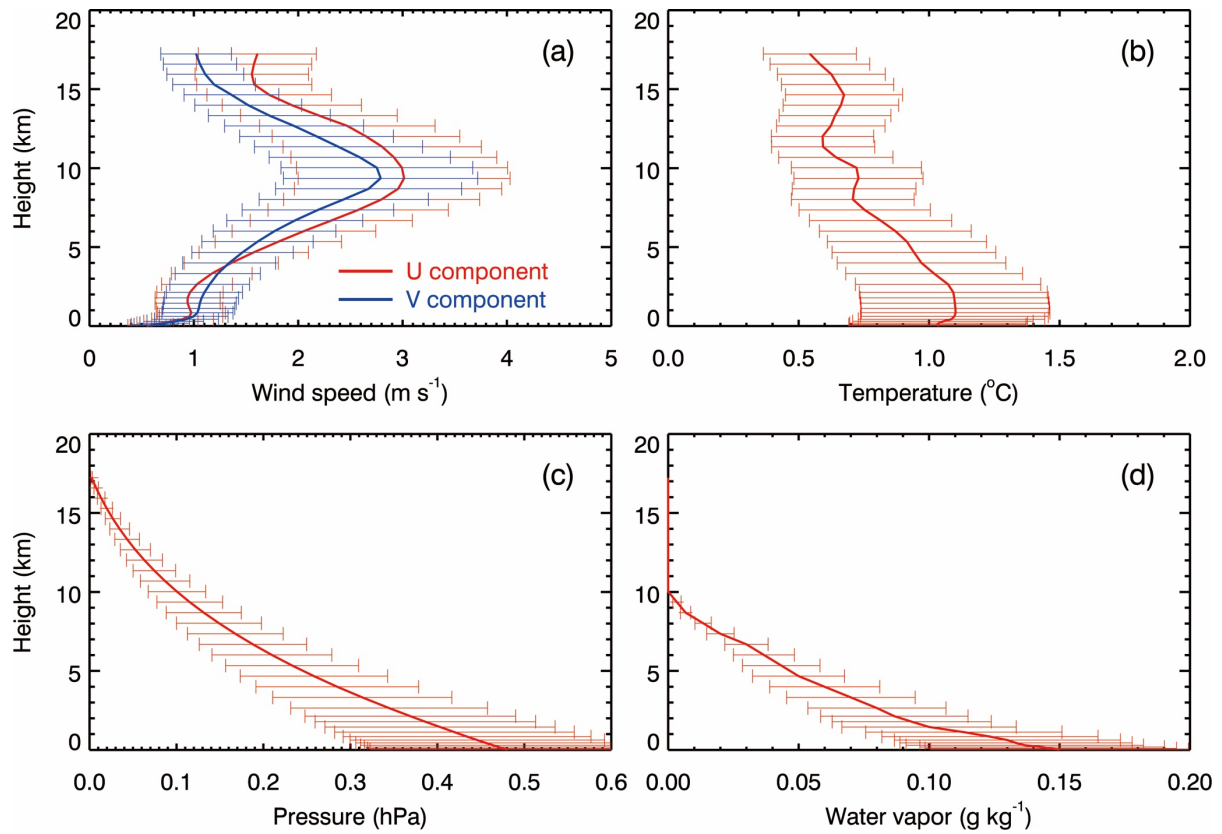


Figure 2 Vertical distribution of the mean of initial ensemble spreads and the standard deviation for (a) horizontal winds (U and V components), (b) temperature, (c) pressure, and (d) water vapor mixing ratio.

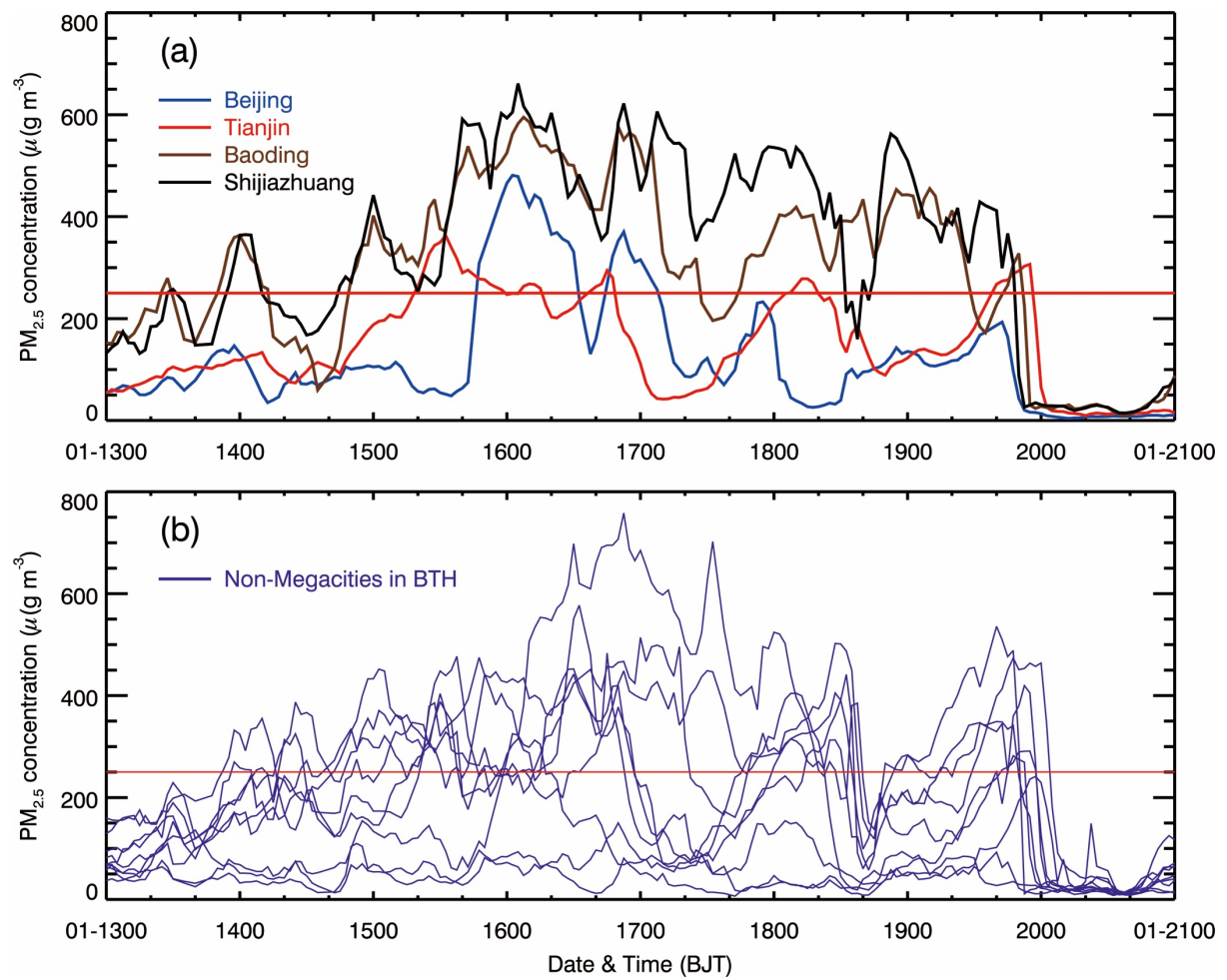


Figure 3 Observed hourly $PM_{2.5}$ concentrations averaged in (a) four megacities (including Beijing, Tianjin, Baoding, and Shijiazhuang) and (b) nine non-megacities of BTH during the period from January 13 to 20, 2014.

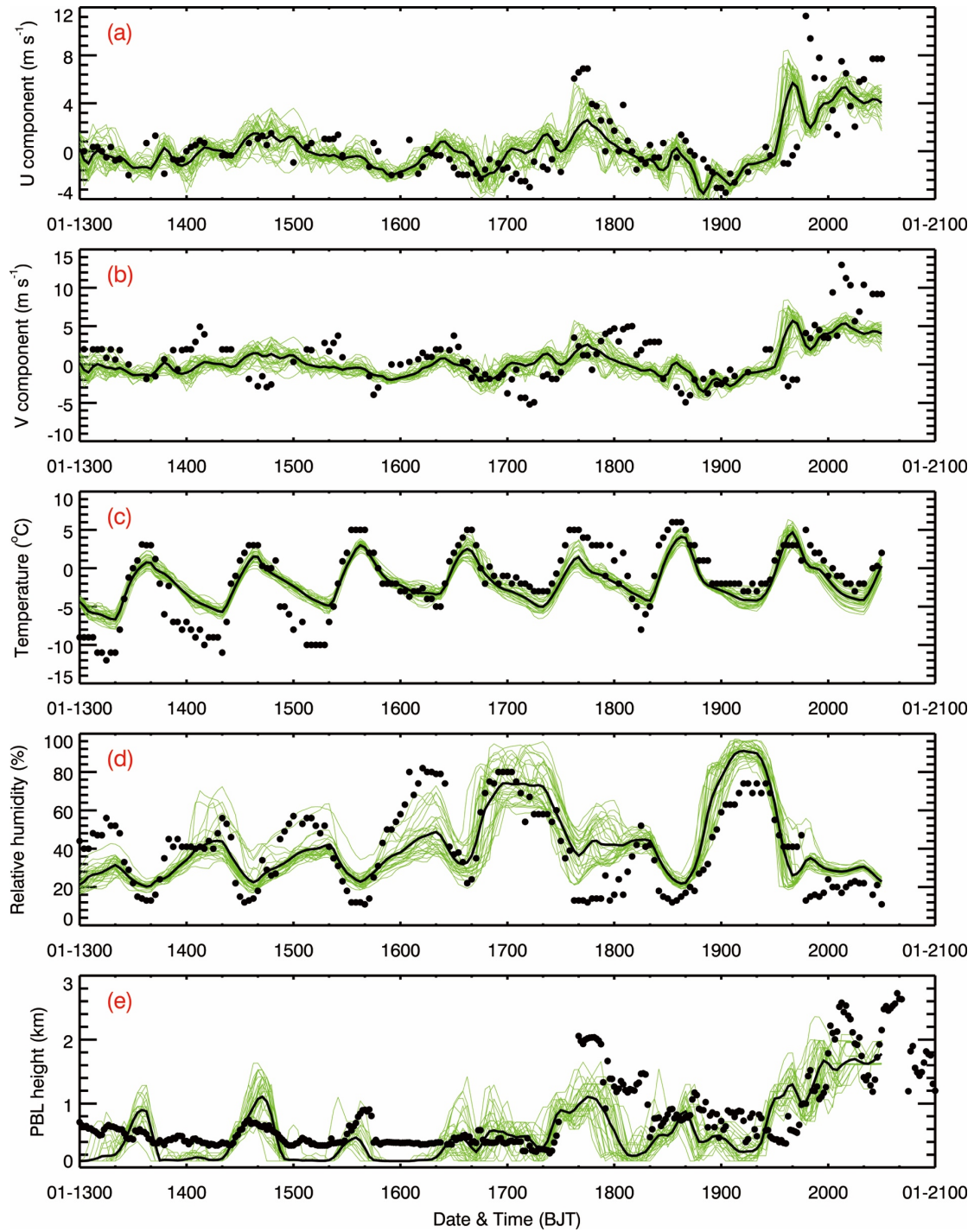


Figure 4 Temporal evolution of the surface (a) U component, (b) V component, (c) temperature, and (d) relative humidity at the meteorological site, and (e) the PBL height at IRSDE in Beijing from each ensemble member (thin green lines), the ensemble mean (bold black line), and observations (black dots) from January 13 to 20, 2014.

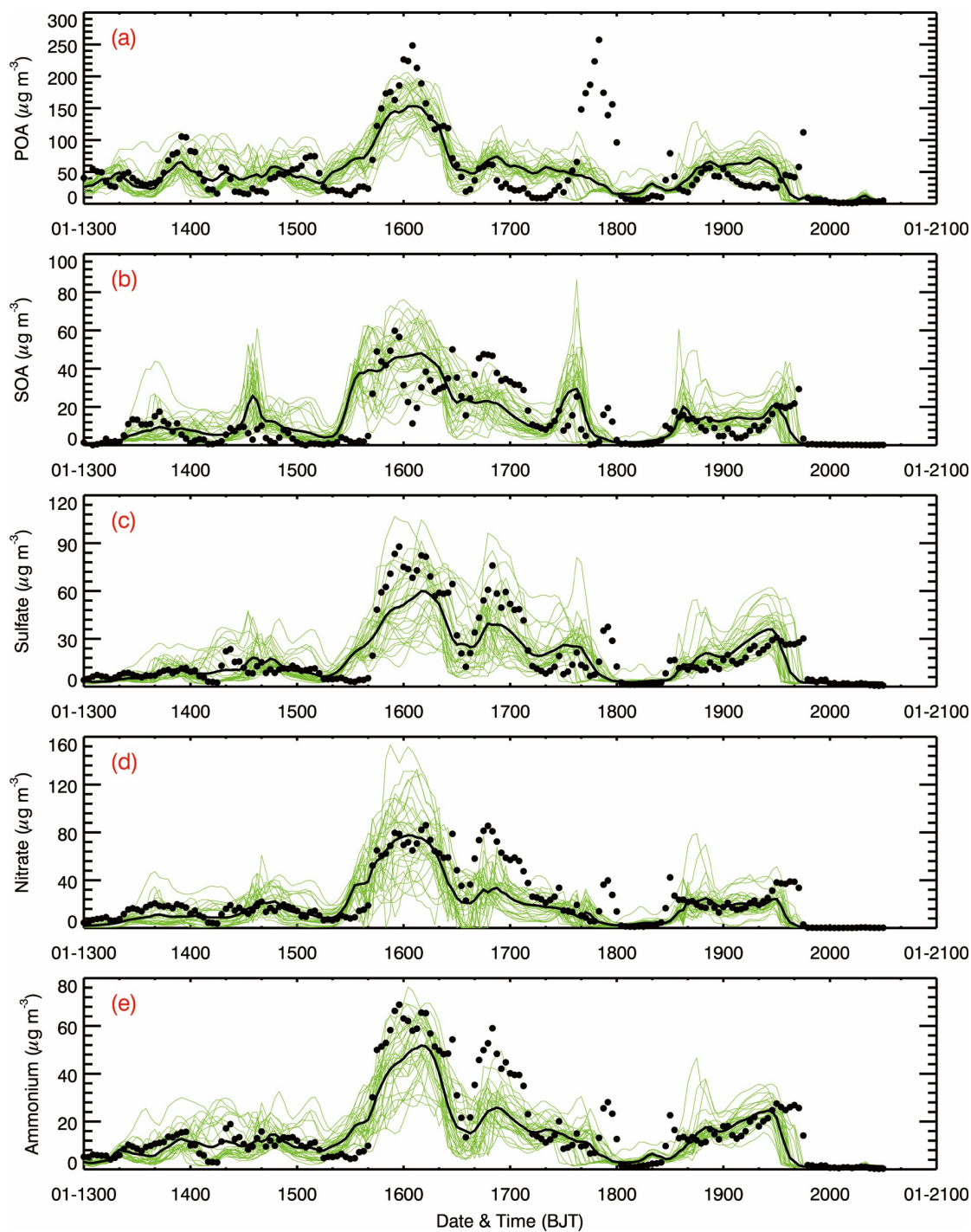


Figure 5 Temporal evolution of the (a) POA, (b) SOA, (c) sulfate, (d) nitrate, and (e) ammonium mass concentrations at IRSDE in Beijing from each ensemble member (thin green lines), the ensemble mean (bold black line), and observations (black dots) from January 13 to 20, 2014.

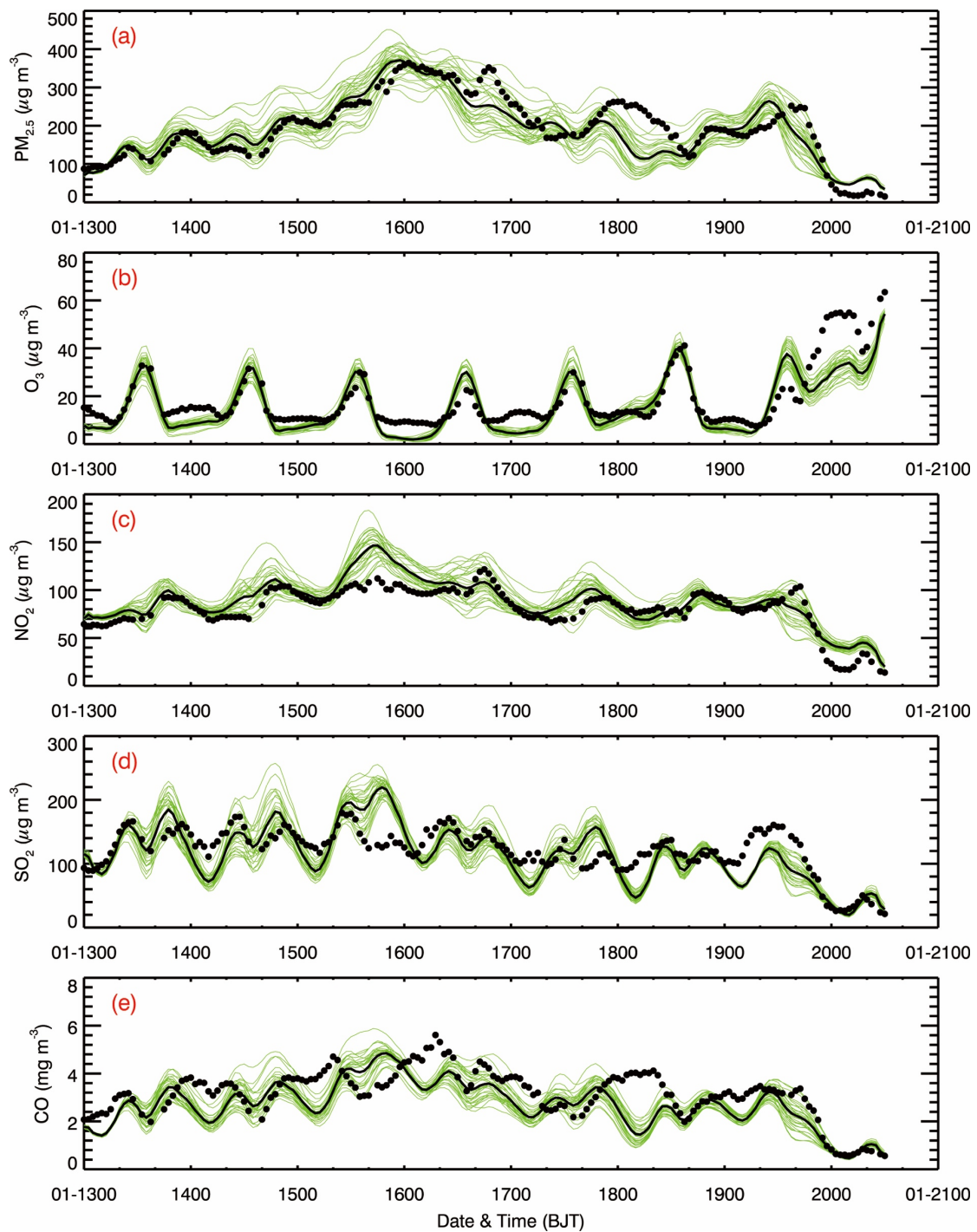


Figure 6 Temporal evolution of the (a) $\text{PM}_{2.5}$, (b) O_3 , (c) NO_2 , (d) SO_2 , and (e) CO mass concentrations averaged over monitoring sites in BTH from each ensemble member (thin green lines), the ensemble mean (bold black line), and observations (black dots) from January 13 to 20, 2014.

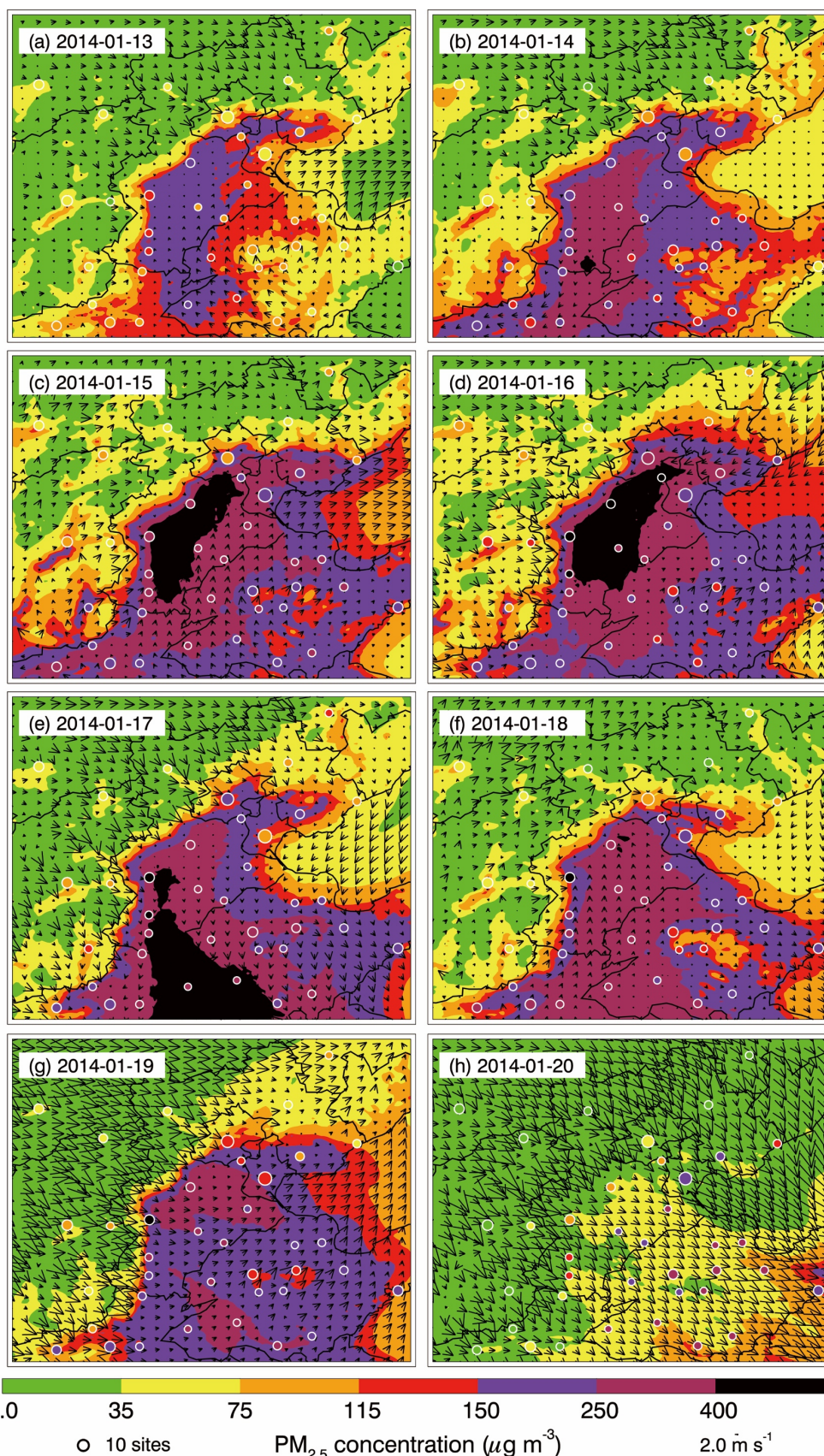


Figure 7 ENSM of the daily average surface $PM_{2.5}$ concentration distributions (colored contour) along with the ENSM of the daily average surface winds (black arrows) from January 13 to 20, 2014. The colored circles denote the $PM_{2.5}$ measurements in cities.

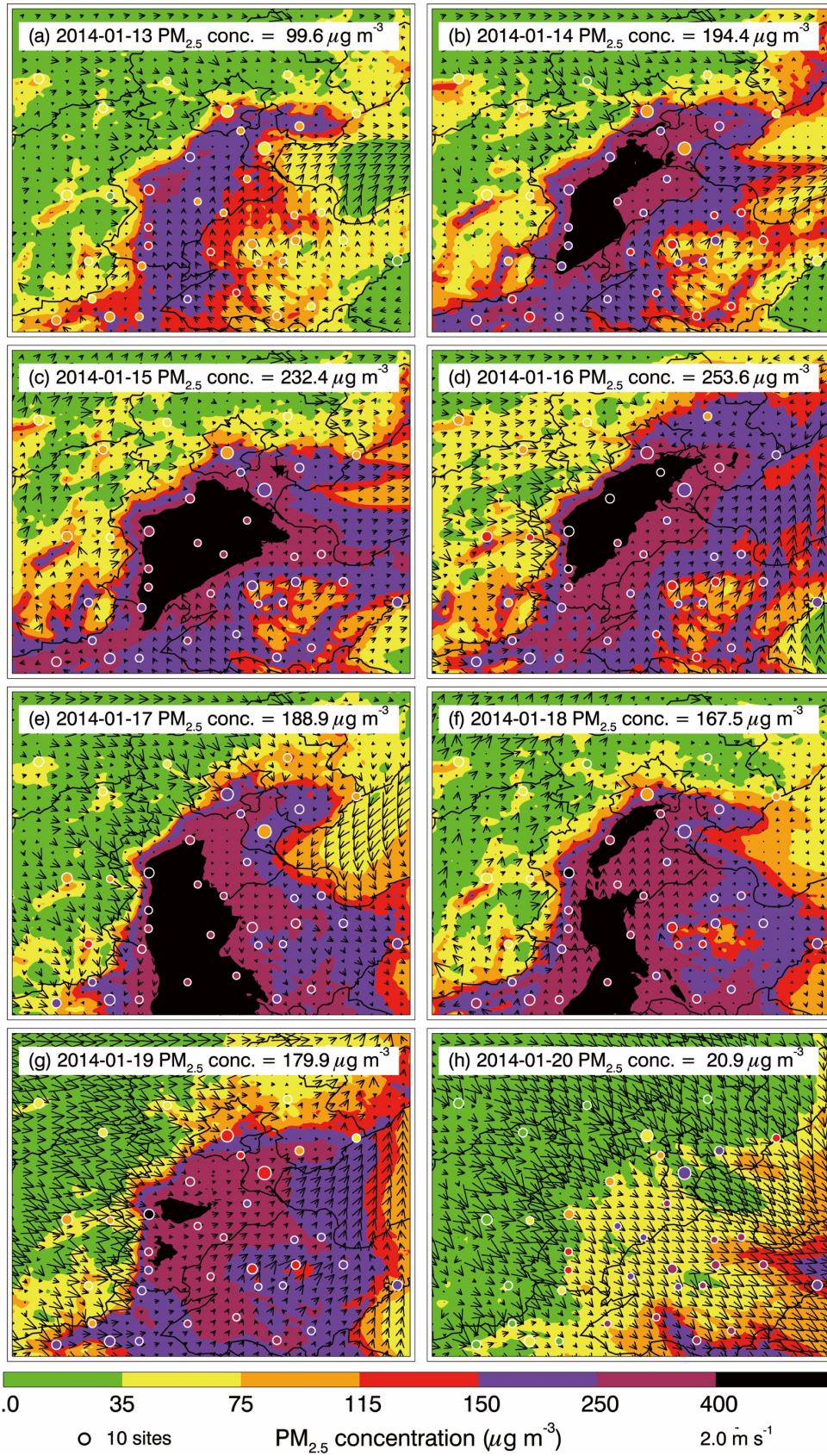


Figure 8 Same as Figure 7, but for the ensemble member of 16 with the highest simulated $\text{PM}_{2.5}$ concentration.

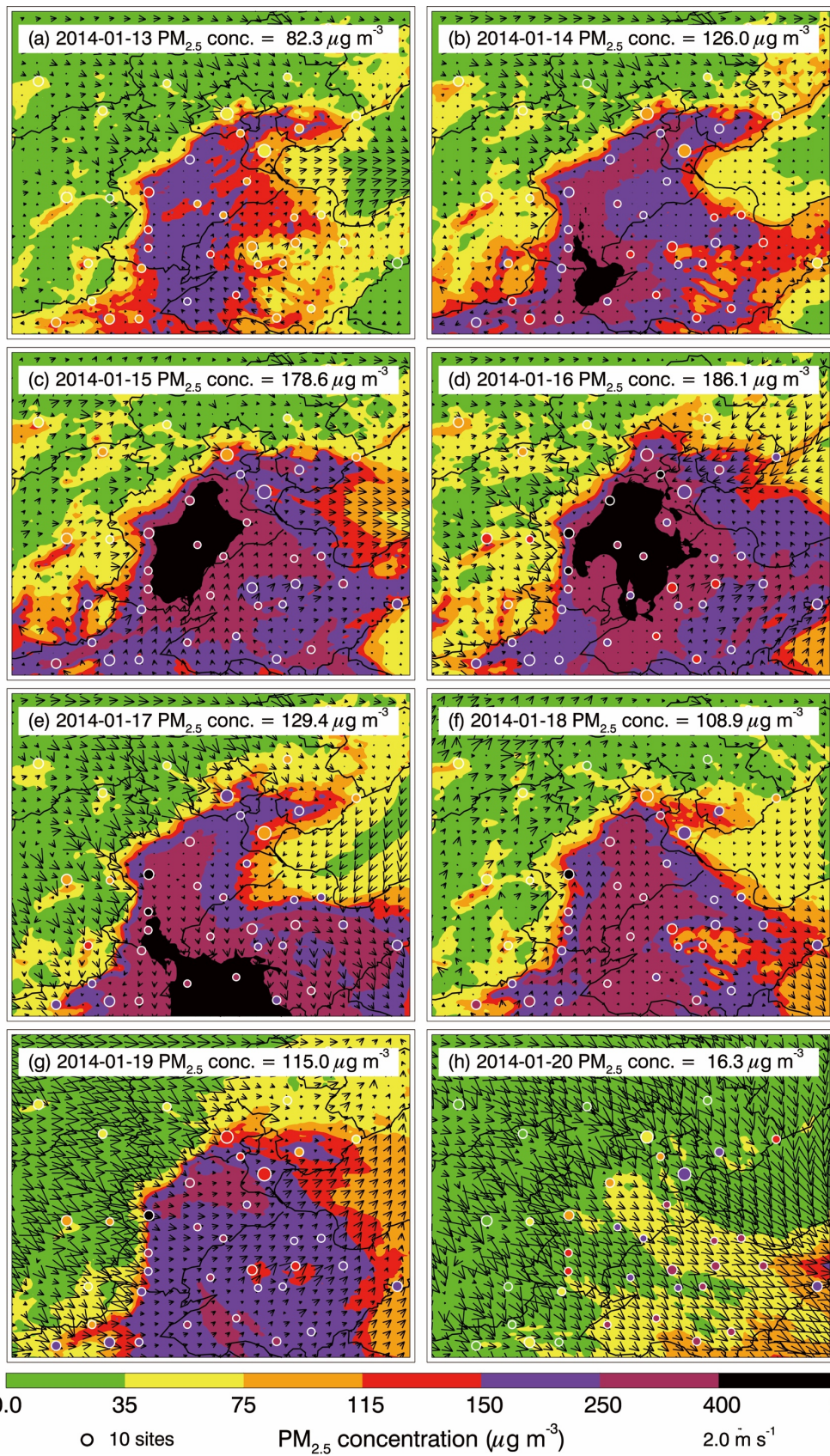


Figure 9 Same as Figure 7, but for the ensemble member of 30 with the lowest simulated $\text{PM}_{2.5}$ concentration.

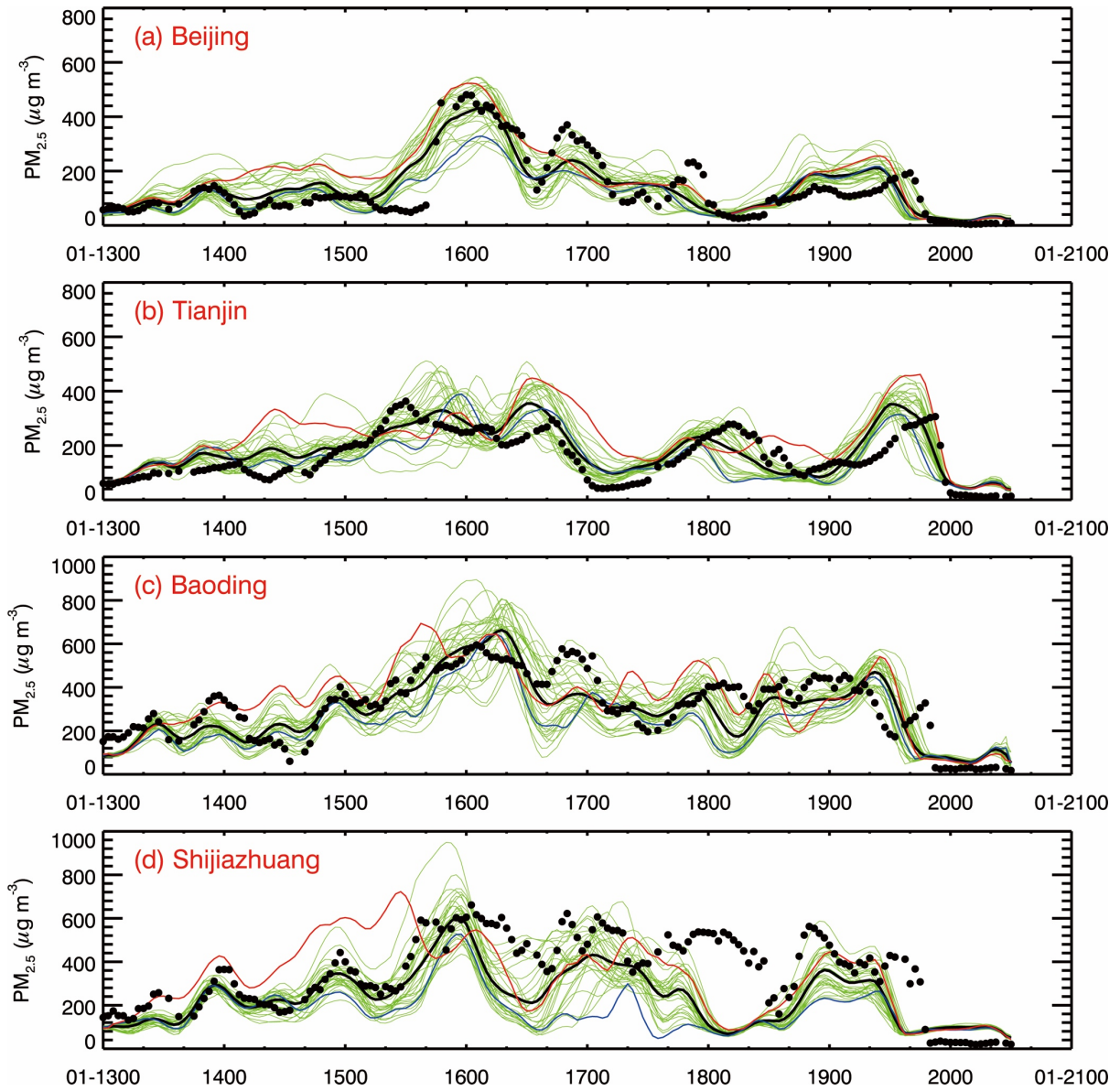


Figure 10 Temporal evolution of the $PM_{2.5}$ mass concentrations averaged in (a) Beijing, (b) Tianjin, (c) Baoding, and (d) Shijiazhuang from each ensemble member (thin green lines), the ensemble mean (bold black line), and observations (black dots) during the period from January 13 to 20, 2014. The red and blue lines represent the simulations in the members with highest and lowest $PM_{2.5}$ concentrations, respectively.